NEOPLASIA
www.neoplasia.com

Volume 15 Number 5 May 2013 pp. 554–567 554

IGFBP-4 Anti-Angiogenic and Anti-Tumorigenic Effects Are Associated with Anti–Cathepsin B Activity[1]

María J. Moreno*, Marguerite Ball*, Marina Rukhlova*, Jacqueline Slinn*, Denis L'Abbe†, Umar Iqbal*, Robert Monette*, Martin Hagedorn‡,§, Maureen D. O'Connor-McCourt†, Yves Durocher† and Danica B. Stanimirovic*

*National Research Council of Canada, Ottawa, Ontario, Canada; †National Research Council of Canada, Montreal, Quebec, Canada; ‡University of Bordeaux, LAMC, UMR 1029, Talence, France; §INSERM, LAMC, UMR 1029, Talence, France

Abstract

Insulin-like growth factor–binding protein 4 (IGFBP-4/IBP-4) has potent IGF-independent anti-angiogenic and anti-tumorigenic effects. In this study, we demonstrated that these activities are located in the IGFBP-4 C-terminal protein fragment (CIBP-4), a region containing a thyroglobulin type 1 (Tg1) domain. Proteins bearing Tg1 domains have been shown to inhibit cathepsins, lysosomal enzymes involved in basement membrane degradation and implicated in tumor invasion and angiogenesis. In our studies, CIBP-4 was shown to internalize and co-localize with lysosomal-like structures in both endothelial cells (ECs) and glioblastoma U87MG cells. CIBP-4 also inhibited both growth factor–induced EC tubulogenesis in Matrigel and the concomitant increases in intracellular cathepsin B (CatB) activity. *In vitro* assays confirmed CIBP-4 capacity to block recombinant CatB activity. Biodistribution analysis of intravenously injected CIBP-4–Cy5.5 in a glioblastoma tumor xenograft model indicated targeted accumulation of CIBP-4 in tumors. Most importantly, CIBP-4 reduced tumor growth in this animal model by 60%. Pleiotropic anti-angiogenic and anti-tumorigenic activities of CIBP-4 most likely underlie its observed therapeutic potential against glioblastoma.

Neoplasia (2013) 15, 554–567

Introduction

The insulin-like growth factor–binding protein (IGFBP) family comprises six related protein members (IGFBP-1 to IGFBP-6) that exhibit high affinity for IGF-1 and IGF-2 [1]. IGFBPs function as carriers of IGFs, prolonging their half-lives and modulating their biologic functions in target cells [1]. In circulation and interstitial fluids, IGFs are tightly associated with IGFBPs and released only after IGFBP proteolysis; this allows the binding of IGFs to plasma membrane IGF receptors through which they exert multiple biologic actions including stimulation of cell proliferation, differentiation, migration, survival, and angiogenesis [2,3]. IGFBPs inhibit these actions by sequestering IGFs away from the receptors. However, some IGFBP members possess heparin-binding domains (HBDs) that facilitate the interaction of the protein with heparin sulfate proteoglycans of the extracellular matrix (ECM), increasing IGF concentration in the proximity of the receptors and thereby enhancing IGF activities [4–6]. In addition, some IGFBPs also have IGF-independent biologic activities [7], although the mechanism(s) of action involved in these specific functions are still not clearly understood.

The IGFBP mature forms are all secreted proteins. IGFBP-4/IBP-4 is the smallest of the six members [8] and can be found both in non-glycosylated (24 kDa) and N-glycosylated (28 kDa) forms [9]. We have previously reported [10] that IGFBP-4 inhibits angiogenesis

Address all correspondence to: María J. Moreno, PhD, National Research Council of Canada, 1200 Montreal Road, Bldg M-54, Ottawa, Ontario, Canada K1A 0R6. E-mail: maria.moreno@nrc.ca

[1]This study was financially supported by the National Research Council Genomics and Health Initiative.

Received 15 January 2013; Revised 12 February 2013; Accepted 15 February 2013

DOI 10.1593/neo.13212

and glioblastoma tumor growth *in vitro*. The anti-angiogenic effect of IGFBP-4 was pleiotropic against multiple angiogens, including IGF-1, vascular endothelial growth factor (VEGF), placenta growth factor, and basic fibroblast growth factor. These inhibitory effects of IGFBP-4 were recently confirmed by Contois et al. [11] using the chick chorioallantoic membrane (CAM) angiogenesis model. In addition, our studies indicated that the anti-tumorigenic effect of IGFBP-4 in the human glioblastoma cell line U87MG is IGF-independent [10]. However, the mechanisms governing these IGF-independent inhibitory effects of IGFBP-4 are not fully understood.

The six IGFBP family members share a highly conserved structure with three major domains, namely, N-terminal domain, central domain, and C-terminal domain, each containing specific subdomains or functional motifs [1]. The N-terminal domain contains important IGF-binding residues that allow for the high-affinity binding of IGF to IGFBPs. The central domain does not exhibit structural similarities among the IGFBP family members; however, sites of N-linked and O-linked glycosylation as well as other sites of posttranslational modification are found in this region [1]. The C-terminal domain contains a thyroglobulin type 1 (Tg1) subdomain; this protein module is present in a number of structurally and functionally unrelated proteins such as thyroglobulin, equistatin, saxiphilin, nidogen, testican-1, the major histocompatability complex (MHC) class II–associated invariant chain, and secreted modular calcium-binding proteins (SMOCs) [12]. Although the role of Tg1 domains has not been fully elucidated yet, the ability of some Tg1 domain–containing proteins to inhibit proteases, primarily cysteine cathepsins, suggests that Tg1 domains may represent a novel group of protease inhibitors [13].

Cathepsins are a large family of proteolytic enzymes responsible for intracellular protein processing and degradation in normal cells. They also play important roles in bone remodeling, epidermal homeostasis, and antigen presentation [14]. Emerging evidence indicates that they are also pivotal players in cancer progression, angiogenesis, and metastasis [15]. Cysteine cathepsins are typically localized in lysosomes and other intracellular compartments; however, in tumors and other activated cells, cathepsins can be translocated to the plasma membrane and, in some cases, secreted into the extracellular space where they participate in the degradation of the ECM components such as laminin, fibronectin, tenascin C, and type IV collagen [16–18], facilitating tumor cell migration and invasion [16,18]. Cathepsins have also been implicated in the activation of other enzymes of the proteolytic cascade that mediate ECM degradation, such as matrix metalloproteases (MMPs) and urokinase plasminogen activator [19]. The human cysteine cathepsin family comprises 11 members (B, C, H, F, K, L, O, S, V, W, and X/Z). Cathepsin B (CatB) specifically has been linked to glioma invasiveness [20] and angiogenesis [21,22] and is a prognostic factor for survival in patients with brain tumors [23].

As previously indicated, the N-terminal sequence of IGFBP-4 contains an IGF-binding domain that is most likely responsible for its IGF-dependent actions. To investigate the IGF-independent mechanisms underlying the anti-angiogenic and anti-tumorigenic effects of IGFBP-4, we focused this study on the C-terminal sequence [IGFBP-4 C-terminal protein fragment (CIBP-4)] that contains a Tg1 domain. We produced recombinant CIBP-4 and demonstrated that this polypeptide retains the pleiotropic anti-angiogenic and anti-tumorigenic properties previously identified in the full-length IGFBP-4 protein. Furthermore, we showed that these effects are associated with its potent anti-CatB activity and that CIBP-4 significantly reduces tumor growth in a xenograft glioblastoma tumor model.

Materials and Methods

Production of Recombinant Full-Length IGFBP-4 and CIBP-4

Full-length IGFBP-4 (IBP-4, Accession number BC016041; MGC: 20162) was amplified with forward (F1: 5′-TAAGAATTCGCCACCATGCTGCCCCTCTGCCT-3′) and reverse (R1: 5′-TTAGGATCCACCTCTCGAAAGCTGTCAGCC-3′) primers, digested with *Eco*RI and *Bam*HI (New England Biolabs, Whitby, Ontario) and cloned in-frame into pTT5SH8Q1 expression plasmid (a smaller version of pTTSH8Q1 vector) containing the C-terminal Steptag-II/$(His)_8$GGQ dual tags [24,25]. The IGFBP-4 C-terminal domain (CIBP-4; nt 155–258) was amplified with forward (F2: 5′-GCCGCTAGCAAGGTCAATGGGGCGCCCCGGGA-3′) and reverse (R1) primers, digested with *Nhe*I and *Bam*HI and ligated in-frame into pYD1 plasmid (pTT5SH8Q1 vector with secreted alkaline phosphatase (SEAP) signal peptide MLLLLLLLGLRLQLSLGIA). Cells were transfected essentially as described [26] with the following modifications: HEK293-6E cells (293-EBNA1 clone 6E) growing as suspension cultures in FreeStyle F17 medium (Life Technologies, Burlington, Ontario) were transfected at 1×10^6 cells/ml. A feed with 0.5% (wt/vol) TN1 peptone (TekniScience, Terrebonne, Quebec) was done 24 hours post-transfection [27]. Culture media were harvested 120 hours post-transfection and IGFBP-4 constructs were purified by sequential affinity chromatography on Fractogel EMD-chelate (EMD-Millipore, Billerica, MA) charged with cobalt [28] followed by StrepTactin-Sepharose as previously described [24]. Purified material was desalted in phosphate-buffered saline (PBS) on D-Salt Excellulose columns (Pierce, Thermo Scientific, Nepean, Ontario) as recommended by the manufacturer. For large-scale CIBP-4 production for animal studies, a 293-6E pool stably expressing CIBP-4 was generated using the pYD7 vector [29] encoding CIBP-4 containing the SEAP single peptide and the C-terminal Steptag-II/$(His)_8$GGQ dual tag (see above). The pool was obtained following transfection of 293-6E cell with pYD7/CIBP-4 plasmid and selection with 5 μg/ml blasticidin (InvivoGen, San Diego, CA) for 3 weeks and 2 μg/ml for another 2 weeks until cells recovered from selection. Blasticidin concentration was then reduced to 0.5 μg/ml for routine cell maintenance. Large-scale CIBP-4 productions were achieved in 10-l or 20-l WAVE bioreactor (GE Healthcare Life Sciences, Baie d'Urfé, Quebec) in F17 medium at 37°C using the manufacturer's recommended conditions. Wave bags were inoculated at 2×10^5 cells/ml and a 0.5% (wt/vol) TN1 feed was performed 3 days post-inoculation. The cultures were typically harvested 8 days post-inoculation (typical cell viability >80%), cells were removed by centrifugation, and clarified medium was concentrated by tangential flow filtration using a 3-kDa Centrasette membrane (Pall Corporation, Mississauga, Ontario). CIBP-4 in the concentrated medium was purified on Fractogel-cobalt as described previously [28] and formulated in PBS. Protein concentration was determined by absorbance at 280 nm using CIBP-4 molar extinction coefficient.

Cell Cultures

Human brain endothelial cells (HBECs) were obtained from small intracortical microvessels and capillary fractions (20–112 μm) harvested from human temporal cortex excised surgically from patients treated for idiopathic epilepsy. Tissues were obtained with approval from the Montreal Neurological Institute Research Ethics Committee. Briefly, cortices were homogenized in Dulbecco's modified Eagle's medium (DMEM) and filtered through a series of Nitex meshes (Sefar

Canada, Saint-Laurent, Quebec) of 350-, 112-, and 20-μm sizes. Vessels from 20-μm mesh were pelleted, digested with collagenase IV (1 mg/ml; Sigma-Aldrich, St Louis, MO) in DMEM (Wisent, St Jean-Baptiste, Quebec) for 5 minutes, and collected by centrifugation. Vessels were then resuspended in media containing DMEM high glucose, 5% heat-inactivated human serum (Sigma-Aldrich), 10% heat-inactivated FBS (HyClone, Logan, UT), 20% medium conditioned murine melanoma cells (mouse melanoma, Cloudman S91, clone M-3, melanin-producing cells purchased from ATCC, Manassas, VA), 5 μg/ml endothelial cell growth supplement (ECGS), insulin-transferrin-selenium premix (final concentrations: 5 μg/ml insulin, 5 μg/ml transferrin, 5 ng/ml selenium; BD Biosciences, Bedford, MA), and 5 units/ml heparin (Sigma-Aldrich), plated on 0.5% gelatin-coated plastic (Sigma-Aldrich) and grown at 37°C in 5% CO_2/95% air. Media were replaced on a 3-day cycle. HBECs were separated from smooth muscle cells with cloning rings at days 10 to 14. Cells were trypsinized weekly at 1:3 split ratio for 8 to 12 passages. HBEC cultures were routinely characterized morphologically and biochemically. More than 95% of cells in culture stained immunopositive for the selective endothelial markers, angiotensin II–converting enzyme and factor VIII–related antigen, incorporated fluorescently labeled acetylated low-density lipoprotein, and exhibited high activities of the blood-brain barrier–specific enzymes, γ-glutamyltranspeptidase and alkaline phosphatase [30].

The human glioma cell line U87MG was derived from human patients diagnosed with grade III astrocytoma and obtained from ATCC. Cells (5×10^4 cells/ml) were plated in poly-L-lysine (25 μg/ml; Sigma-Aldrich) precoated 35-mm dishes and grown at 37°C in DMEM containing 10% FBS (HyClone) in humidified atmosphere of 5% CO_2/95% air. To obtain U87MG conditioned media (CM), cells were grown to 80% confluence in growth media and replaced by serum-free DMEM for 3 days, collected, and filtered (Millex-GV sterilizing filter unit, 0.22 μm; Millipore, Etobicoke, Ontario).

Capillary-like Tube Formation Assay and Intracellular CatB Activity Measurement

In vitro angiogenesis was assessed by endothelial tube formation in a growth factor–reduced basement membrane, Matrigel (BD Biosciences), as previously described [10]. Twenty-four–well plates were coated with 300 μl of unpolymerized Matrigel (7–11 mg protein/ml, diluted 1:2 in DMEM) and allowed to polymerize for 30 minutes at 37°C. HBECs (4×10^4) were suspended in 500 μl of DMEM alone, DMEM containing growth factors (150 ng/ml IGF-I or 20 ng/ml VEGF165; R&D Systems, Minneapolis, MN), or U87MG CM (as described in Cell Cultures section) in the absence or presence of 20 nM IBP-4 or CIBP-4 and plated into Matrigel-coated wells. Capillary-like tube (CLT) formation was analyzed after 24 hours using an Olympus 1X50 microscope. Phase contrast images were captured using a digital video camera (Olympus U-CMT) and analyzed with Northern Eclipse v.5.0 software. Grayscale images were thresholded, converted to binary images, and skeletonized, and the total length and number of nodes (branching points) of the CLT formed by HBECs were quantified. Experiments were performed in duplicate wells and repeated at least four times. To determine the levels of CatB activity in each experimental condition, 260× dilution Magic Red CatB reagent (Immunochemistry Technologies, Bloomington, MN) was added to all wells at the end of the experiment and maintained at 37°C in the dark for 2 hours. Magic Red contains a membrane permeable CatB target sequence peptide (arginine-arginine) linked to an amide-substituted fluorophore, cresyl violet, that upon enzymatic cleavage at the arginine amide linkage site generates red fluorescence. Cells were washed twice with Hank's balanced salt solution (HBSS) and intracellular fluorescence quantification (530-nm excitation and 645-nm emission) was performed using a cytofluorimeter plate reader (Bio-Tek FL600; BioTek Instruments, Inc, Winooski, VT).

In Vitro *Evaluation of CatB Activity*

The ability of CIBP-4 to inhibit the catalytic activity of a recombinant human CatB (rhCatB) enzyme expressed in the NSO murine myeloma cell line (R&D Systems) was evaluated using the fluorogenic peptide substrate, *N*-carbobenzyloxy-Leu-Arg-7-amido-4-methylcoumarin (Z-L-R-AMC; R&D Systems). rhCatB (10 μg/ml) was activated by preincubation in 25 mM 2-(*N*-morpholino)ethanesulfonic acid (JT Baker, Phillipsburg, NJ) and 5 mM DL-dithiothreitol (Sigma-Aldrich) at pH 5.0 for 15 minutes at room temperature. Active rhCatB (10 ng) alone or in the presence of either CIBP-4 (0.1–10 μM) or the synthetic CatB inhibitor Ca-074 ME (0.1–10 μM; Calbiochem, La Jolla, CA) was added to Z-L-R-AMC (50 μM) in 25 mM 2-(*N*-morpholino)ethanesulfonic acid (pH 5.0). Fluorescence released by the cleavage of Z-L-R-AMC was measured at 37°C every 5 minutes for a total of 60 minutes using a cytofluorimeter plate reader with excitation and emission wavelengths of 380 and 460 nm, respectively.

Anchorage-dependent and Anchorage-Independent U87MG Cell Growth

Anchorage-dependent U87MG cell growth was evaluated using the CyQUANT Cell Proliferation Assay Kit (Molecular Probes, Eugene, OR) following the manufacturer's protocol as previously described [31]. HBECs were plated in quadruplicate in 96-well plates at a density of 3000 cells/well. Cells were grown in phenol red–free DMEM (Life Technologies) + 1% FBS alone or in the presence of 20 nM IBP-4, 20 nM CIBP-4, or 500 μM dibutyryladenosine cyclic monophosphate (dB-cAMP; positive control; Sigma-Aldrich). Treatments were reapplied at day 3. Plates were harvested at 2, 3, 5, and 6 days by gently removing media, blotting the microplates dry, and storing at −80°C until analysis. Plates were thawed at 21°C and 200 μl of CyQUANT GR dye/lysis buffer was added to each well for 5 minutes in the dark. Fluorescence values were measured using a cytofluorimeter plate reader at 485-nm excitation and 530-nm emission, and cell numbers were derived from a standard curve. Experiments were repeated three times.

Anchorage-independent U87MG cell growth was evaluated in semisolid agar in the absence or presence of either 20 nM IBP-4 or CIBP-4 as described previously [10]. Approximately 1800 cells ± treatment were resuspended in 150 μl of growth medium (DMEM + 10% FBS) containing 0.6% agar (Quelab, Montreal, Quebec) and seeded into a well of a 24-well plate previously layered with 250 μl of 0.6% agar. The solidified cell layer was covered with 50 μl of DMEM ± treatment that was replaced every 3 days over a 14-day period. Phase contrast images (six fields per well) were captured using a digital video camera (Olympus U-CMT) and analyzed with Northern Eclipse v.5.0 software. Color images were transformed to grayscale, thresholded, and then converted to binary images. Number and area of colonies per field were calculated. To measure cell viability, at the end of the experiment, 50 μl of Alamar Blue (Cedarlane, Burlington, Ontario) was added to each well and fluorescence readings (530-nm excitation and 590-nm emission) were performed every 10 minutes

for a period of 180 minutes. Experiments were repeated four times in triplicates.

Conjugation of Alexa Fluor 647 to IGFBP-4 and CIBP-4 Protein Fragments

Eighty microliters of 1 mM Alexa Fluor 647 (AF647) succinimidyl ester (Molecular Probes) in DMSO was added to 0.4 ml of 0.2 mg/ml IBP-4 or CIBP-4 recombinant proteins in 100 mM carbonate (pH 8.4), and samples were incubated overnight at room temperature. The reactions were stopped with 150 μl of 200 mM ethanolamine (pH 8.0). To remove free AF647 dye, samples were diluted with 4.5 ml of water and loaded onto 1 ml of Co^{2+}-Talon Metal Affinity column (Pierce, Thermo Scientific) equilibrated with PBS. The column was exhaustively washed with PBS and the labeled proteins were eluted with 2 ml of 1 M imidazole in PBS. To remove imidazole from labeled protein and peptides, the sample was concentrated to approximately 200 μl on Biomax (molecular weight cutoff, 5000; Thermo Scientific, Nepean, Ontario), diluted to original volume with PBS, and concentrated again. The process of concentration/dilution was repeated three times. The final volume was 0.5 ml (0.14 mg/ml). Recovery was between 84% and 87%.

Confocal Laser Scanning Microscopy

Internalization of AF647-conjugated CIBP-4 in HBECs and U87MG cells was analyzed by confocal laser scanning microscopy. HBECs (30,000) and U87MG (50,000) cells were, respectively, seeded on human fibronectin (50 μg/ml; BD Biosciences) or poly-L-lysine–coated coverslips in HBEC or U87MG media at 37°C and grown to 80% confluence. Cells were washed twice with HBSS and incubated in DMEM for 15 minutes at 37°C before the addition of 200 nM AF647–CIBP-4 for up to 4 hours. Images were collected at 90 minutes after removing the fluorescent peptides by washing the cells three times with HBSS.

To determine co-localization of the fluorescently tagged peptides with lysosomes in HBEC, cells were incubated with DMEM containing 200 nM AF647-peptide conjugate and 150 nM LysoTracker Yellow HCK-123 (Molecular Probes) for 90 minutes and then washed with HBSS. Cells exposed were counterstained with the membrane dye Merocyanine 540 (10 μM; Sigma-Aldrich) for 15 minutes and then washed with HBSS.

To determine whether CIBP-4 can inhibit CatB activity in U87MG cells, the cells were incubated with DMEM containing 200 nM unlabeled CIBP-4 for 75 minutes, and then 520× dilution of Magic Red CatB detection solution was added for an additional 15 minutes. The cells were counterstained with the membrane dye DiOC5(3) (500 nM; Molecular Probes) for 30 seconds and then washed with HBSS. Imaging of cells was performed using a Zeiss LSM 410 (Carl Zeiss, Thornwood, NY) inverted laser scanning microscope equipped with an argon/krypton ion laser and a Plan-Apochromat 63×, NA 1.4. Confocal images of two fluoroprobes were sequentially obtained using 488-nm excitation and 515- to 540-nm emission to detect both DiOC5(3) and LysoTracker Yellow HCK-123 fluorescence, 568-nm excitation and 575- to 640-nm emission to detect both Merocyanine 540 and Magic Red CatB fluorescence, and 647-nm excitation and 670- to 810-nm emission to detect AF647 fluorescence.

CAM Experimental Glioma Assay

The ability of CIBP-4 to inhibit glioblastoma tumor growth was assessed in tumor model in chick embryos (U87MG cell grafted on the CAM) as previously described [32,33].

Fertilized chicken (*Gallus gallus*) eggs were obtained from Canadian Food Inspection Agency and placed into an egg incubator at 37°C and 67% to 70% humidity (day 0). At day 3, windows were cut in the

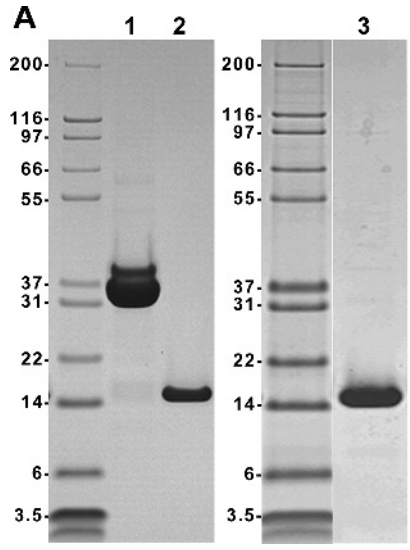

Figure 1. Production of IBP-4 and CIBP-4 in HEK293 cells. (A) IBP-4 (lane 1; 7.5 μg loaded) and CIBP-4 (lane 2; 3.5 μg loaded) proteins were generated by large-scale transfection of HEK293 cells and purified by immobilized metal affinity chromatography on Fractogel-cobalt column, followed by a second affinity purification on StrepTactin-agarose. For large-scale CIBP-4 production for animal studies, a HEK293 pool stably expressing the protein was generated and grown in 10-l WAVE bioreactor. The secreted CIBP-4 protein was purified by immobilized metal affinity chromatography only (lane 3; 2.5 μg loaded). Proteins were resolved by reducing sodium dodecyl sulfate–polyacrylamide gel electrophoresis and stained by Coomassie Blue R-250. (B) Amino acid sequence of IBP-4 and CIBP-4. The signal peptides are underlined, whereas the Steptag-II/$(His)_8$GGQ tags are italicized. The three amino acids in bold (IAS) shown in CIBP-4 sequence are derived from the SEAP.

eggshell and covered with protective surgical Durapore tape until day 10. Then, a sterile plastic ring was placed onto the CAM, the delimited surface carefully scraped with a scalpel blade, and a pellet of 10^6 U87MG cells deposited into the center of the ring. From days 11 to 14, 30 µl of either 3% DMSO alone (vehicle) or in combination with 108 ng of CIBP-4 was topically applied over the tumor each day. At day 17, the tumors were isolated from the CAM and weighed.

Frequency distribution of the tumor population between vehicle-treated and CIBP-4–treated groups was analyzed for three size intervals using Chi-square test.

Subcutaneous Xenograft Tumor Model

CD-1 nude mice (male, 6–8 weeks old) were purchased from Charles River Canada (Saint Constant, Quebec). The animals were housed in cages, in groups of three to five, and maintained on a 12-hour light/dark schedule with a temperature of 22°C and a relative humidity of 50 ± 5%. Sterilized food and water was available *ad libitum*. Experiments were approved by the National Research Council Canada (NRCC) Animal Care Committee in accordance with Canadian Council on Animal Care guidelines. For subcutaneous tumor implantation, mice underwent light isoflurane anesthesia, and 3×10^6 U87MG tumor cells per 50 µl of Matrigel (dilution 1:1 in saline) were injected subcutaneously in the left flank of the mice using a 300-µl syringe. The size of the tumors was monitored with a caliper. Tumor volume was calculated using the formula (length × width^2)/2. When the tumors reached a volume of ~100 mm^3, initiating the exponential growth phase, animals were intravascularly (i.v.) administered with either vehicle or 10 mg/kg CIBP-4 three times per week. Animals were sacrificed when tumors reached ~2500 mm^3.

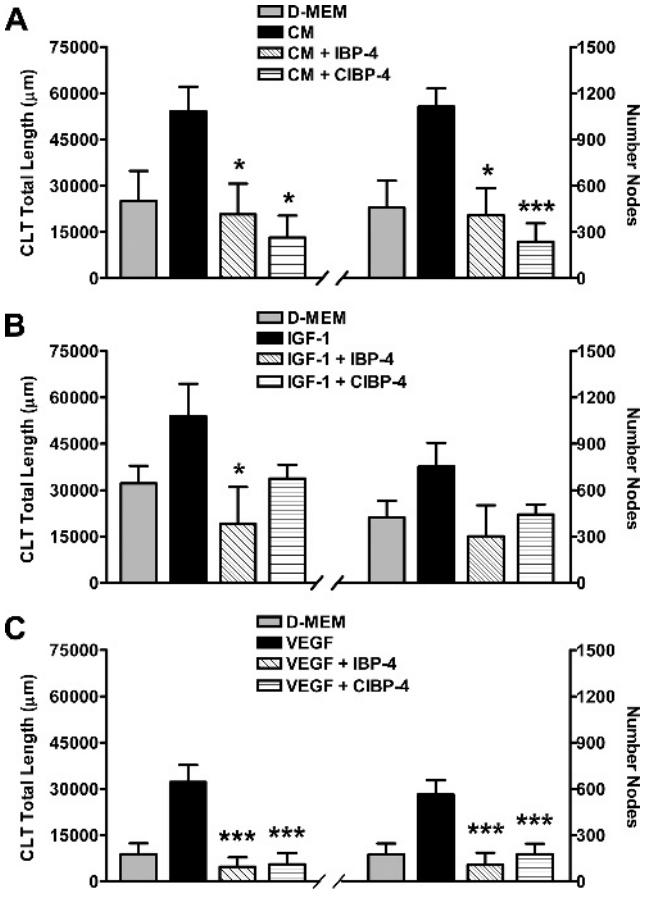

Figure 2. Effects of IBP-4 and CIBP-4 on growth factor–induced CLT formation by HBEC grown in Matrigel. Histograms representing total length (left panels) and number of branching nodes (right panels) of CLT networks. HBECs were exposed to DMEM, U87MG CM, 150 ng/ml IGF-1, or 20 ng/ml VEGF in the absence (black bars) or presence (hatched bars) of either 20 nM IBP-4 or CIBP-4. Bars are means ± SEM of four to seven experiments; * and *** indicates significant difference ($P < .05$ and $P < .001$, respectively) between growth factor–treated HBEC in the absence or presence of IBP-4/CIBP-4. Significance was determined by analysis of variance (ANOVA) followed by Dunnett's multiple comparison test.

In Vivo *Near-Infrared Fluorescence Imaging*

CIBP-4 was labeled with Cy5.5 succinimidyl ester using methods recommended by the manufacturer (GE Healthcare, Mississauga, Ontario). Labeling was optimized to achieve a dye/antibody ratio of 1. U87MG subcutaneous tumor-bearing animals were i.v injected (via tail vein) with 100 µg of CIBP-4–Cy5.5 and imaged at multiple time intervals (0.5, 1, 2, 4, and 24 hours) using a small-animal time-domain eXplore Optix MX2 Preclinical Imager (Advanced Research Technologies, Montreal, Quebec) as previously described [34]. In all imaging experiments, a 670-nm pulsed laser diode with a repetition frequency of 80 MHz and a time resolution of 12-ps light pulse was used for excitation. The fluorescence emission at 700 nm was collected by a highly sensitive time-correlated single-photon counting system and detected through a fast photomultiplier tube. The data were recorded as temporal point-spread functions and the images were reconstructed as fluorescence concentration maps using ART Optix Optiview analysis software 2.0 (Advanced Research Technologies). At the end of the imaging, animals were injected with 40 µg of fluorescein-labeled tomato lectin (Vector Laboratories, Burlingame, CA) to stain blood vessels, then sacrificed 10 minutes later by transcardial perfusion with saline under deep anesthesia. The tumors were excised and fixed overnight in formalin and then sectioned with a viibratome (Ted Pella, Redding, CA). Tissue sections were mounted on Superfrost Plus microscope slides (Fisher Scientific, Nepean, Ontario) using mounting media containing 2 µg/ml 4′,6-diamidino-2-phenylindole, dihydrochloride (DAPI) nuclei stain (Sigma-Adrich). Sections were then visualized under an Olympus 1X 81 inverted motorized microscope (Olympus, Markham, Ontario). InVivo and ImagePro 6.2 software (Olympus) were used to acquire and analyze images.

Pharmacokinetic Profile of CIBP-4

CIBP-4–Cy5.5 (300 µg) was injected through the tail vein in CD-1 mice and subjected to fluorophore-based pharmacokinetic analysis as described previously [34]. After CIBP-4–Cy5.5 injection, blood samples (50 µl) were collected into ice-stored heparin-coated tubes at different time points (0, 0.5, 1, 1.5, 2, and 4 hours) from a small nick produced in the tail vein. Levels of CIBP-4–Cy5.5 were quantified in the blood samples using a fluorescent plate reader with 670-nm excitation and 690-nm emission. The concentration of protein in each sample was derived from standard curves consisting of a range of concentrations of the labeled proteins diluted in mouse blood. Pharmacokinetic parameters were calculated using the WinNonlin pharmacokinetic software package version 5.2 (Pharsight Corporation, Sunnyvale, CA).

A two-compartment IV bolus model was selected for pharmacokinetic modeling, because it best represented the data and route of administration. This model is described by the following equation: $C(t) = A\exp(-\alpha t) + B\exp(-\beta t)$, where $C(t)$ represents the concentration of agent in serum, A and B represent the zero time intercept of the α phase and β phase, respectively, and α and β are disposition rate constants, $\alpha > \beta$. The area under the serum concentration–time curve (AUC) was calculated with the equation AUC0-∞ = D/V/K10, where D is the dose given, V is the apparent distribution volume, and K10 is the elimination rate constant. Total clearance was determined from the equation Cl/F = D/AUC0-∞.

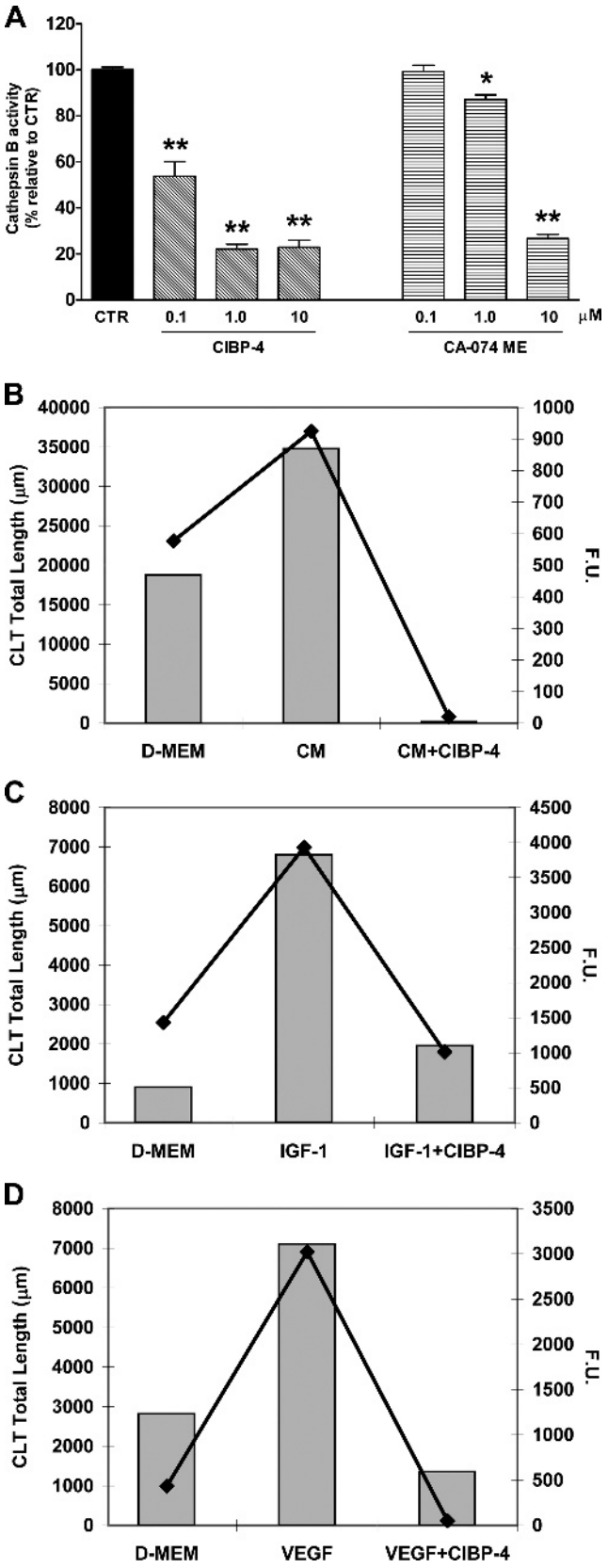

Results

Production of Recombinant IBP-4 and CIBP-4 Protein Fragments

Full-length (IBP-4) and C-terminal (CIBP-4) constructs bearing a dual C-terminal Streptag-II and polyhistidine tag were expressed in HEK293 cells and purified by affinity chromatography. The transient expression of both constructs in HEK293 cells followed by sequential affinity chromatography on Fractogel-cobalt followed by StrepTactin-agarose typically generated 5 to 10 mg of purified protein per liter of culture (Figure 1*A*, lanes 1 and 2). Due to the large amounts of recombinant protein needed for conducting animal studies, we generated a stable HEK293 pool expressing CIBP-4. From a 10-l batch culture and following a single Fractogel-cobalt affinity capture, between 200 and 350 mg was typically obtained (Figure 1*A*, lane 3).

IBP-4 and CIBP-4 Inhibit HBEC CLT Formation in Matrigel

Angiogenic responses induced by U87MG CM and growth factors (IGF-1 and VEGF) on HBEC seeded in Matrigel were evaluated by the total length and the number of nodes/branching points of the CLT networks formed. A tight correlation in the pattern of changes between CLT total length (Figure 2, *left panels*) and number of nodes (Figure 2, *right panels*) was obtained for each individual experiment.

HBEC exposed to DMEM showed a variable response ranging from no angiogenic activity (flat cells, no tubulogenesis) to a restricted spontaneous angiogenic activity (sprouting with minimal tube formation and connectivity; Figure 2, *A*–*C*). U87MG CM (Figure 2*A*) and the growth factors IGF-1 (Figure 2*B*) and VEGF165 (Figure 2*C*), respectively, induced ~2.2-, 1.8-, and 3.6-fold increase in both HBEC CLT total length and node number compared to DMEM. IBP-4 (20 nM) and CIBP-4 (20 nM) blocked the angiogenic responses induced by U87MG CM and both growth factors were tested (Figure 2, *A*–*C*), keeping HBEC responses at spontaneous angiogenic levels.

Figure 3. Effect of CIBP-4 on CatB activity. (A) Histogram representing the *in vitro* proteolytic activity of human recombinant CatB protein (10 ng) in the absence or presence of either CIBP-4 (0.1–10 μM) or the synthetic CatB inhibitor CA-074 ME (0.1–10 μM). Bars are means ± SEM of three experiments (n = 9). *P < .05 and **P < .0001 indicates significant difference between active rhCatB alone or in the presence of the treatments as determined by ANOVA followed by Dunnett's multiple comparison test. (B–D) Representative graphs of a single experiment showing CLT total length (bars; left Y axis) and intracellular CatB activity (line plot; right Y axis) by HBEC seeded in Matrigel and exposed to DMEM (B–D), U87MG CM (B), 150 ng/ml IGF-1 (C), or 20 ng/ml VEGF (D) in the absence or presence of CIBP-4 (20 nM). CatB activity was monitored using Magic Red CatB reagent. Experiments were repeated four times. F.U., fluorescence units.

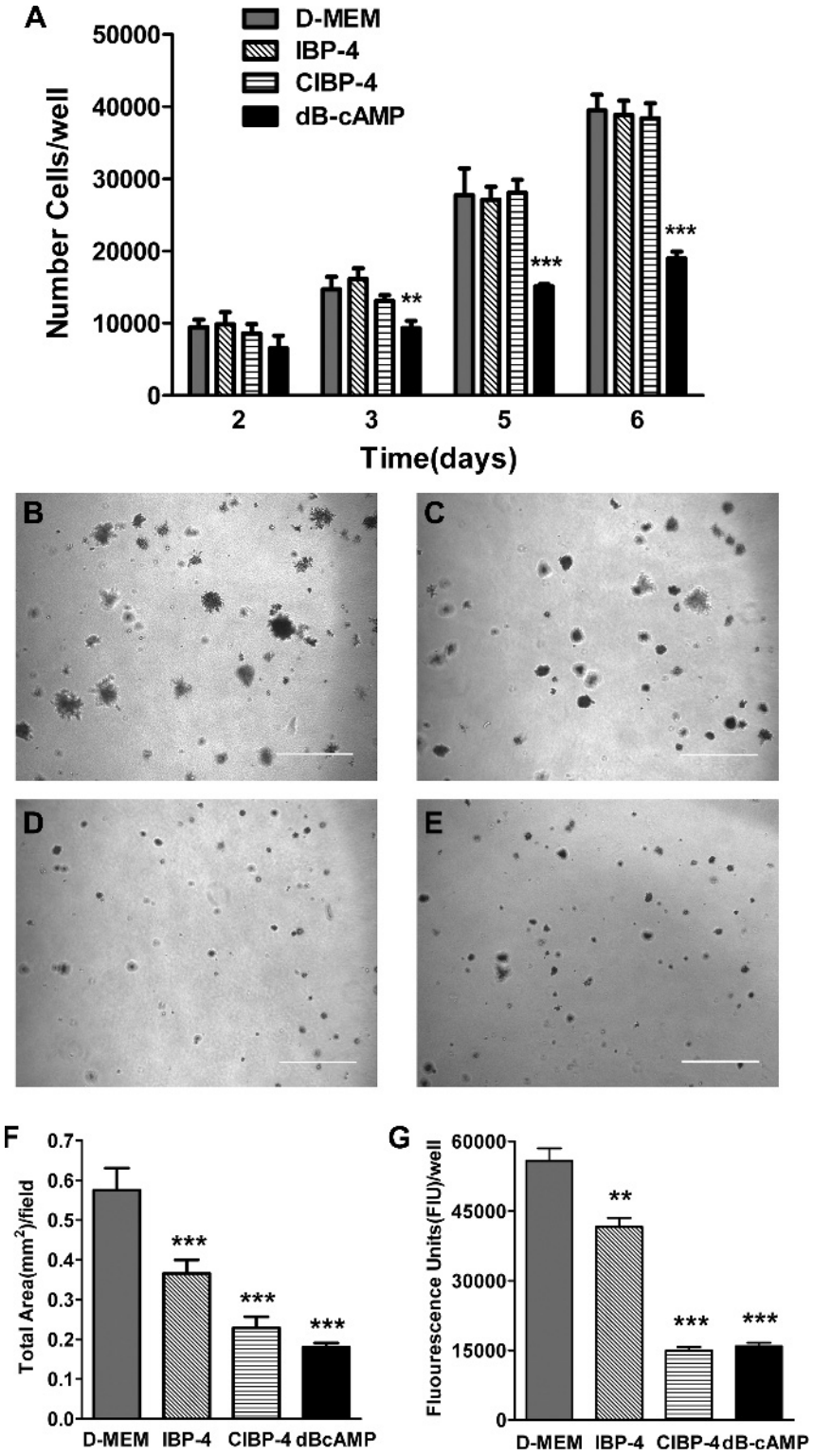

Figure 4. Effects of IBP-4 and CIBP-4 on U87MG anchorage-dependent and anchorage-independent growth. (A) Histogram representing anchorage-dependent growth of U87MG cells in the absence (gray bars) or presence (hatched bars) of 20 nM IBP-4, 20 nM CIBP-4, or 500 μM dB-cAMP (positive control, black bars) over 6 days. (B–E) Representative images of anchorage-independent growth of U87MG cells in soft agar in the absence (B) or presence of 20 nM IBP-4 (C), 20 nM CIBP-4 (D), or 500 μM dB-cAMP (E) for 2 weeks. Calibration bar, 500 μm. (F and G) Histograms representing quantitative analysis of U87MG cell growth in soft agar by the total covered area per field (F) and cellular metabolic activity measured by Alamar blue (G). Each bar represents mean cell number per well ± SEM [$n = 4$ (A), $n = 10$ (F), $n = 3$ (G)]. Asterisks indicate significant (**$P < .01$ and ***$P < .001$) differences between DMEM and treatments as determined by ANOVA followed by either Newman-Keuls multiple comparison test (A) or by Dunnett's multiple comparison test (F and G).

CIBP-4 Inhibits CatB Activity In Vitro

The inhibitory capacity of CIBP-4 against the peptidolytic activity of recombinant CatB was assessed by monitoring the cleavage of the fluorogenic substrate Z-L-R-AMC immediately after exposure to the peptide. CIBP-4 induced a concentration-dependent inhibitory effect on CatB activity ranging from ~46% (at 0.1 μM) to ~78% (at both 1 and 10 μM; Figure 3*A*). The permeable synthetic CatB inhibitor CA-074 ME was ineffective at 0.1 μM and reduced CatB activity by ~13% and ~73% at 1 and 10 μM, respectively. CIBP-4 was significantly more potent than CA-074 ME at 0.1 and 1 μM concentrations and equally effective at 10 μM (Figure 3*A*).

Incubation of CIBP-4 with activated CatB did not produce CIBP-4 cleavage products as analyzed by sodium dodecyl sulfate–polyacrylamide gel electrophoresis (data not shown), thereby excluding the possibility that CIBP-4 could act as a competitive substrate for the enzyme in this assay.

CIBP-4 Inhibits CatB Activity Induced in Angiogenic HBEC in Matrigel

To assess intracellular CatB activity levels in HBEC seeded in Matrigel and exposed to various growth factors in the absence or presence of CIBP-4, the cleavage of a membrane permeable CatB target sequence peptide (Magic Red CatB reagent) was monitored at the end of the angiogenesis assay.

The levels of intracellular CatB activity in HBEC exposed to DMEM alone were variable between experiments and did not consistently correlate with the levels of spontaneous angiogenic activity (CLT total length) exhibited by the cells (Figure 3, *B–D*). U87MG CM, IGF-1, and VEGF, respectively, induced ~1.9-, ~7.5-, and ~2.5-fold increases in HBEC angiogenic response compared to DMEM alone (Figure 3, *B–D*). This correlated with an induction of intracellular CatB activity of ~1.6-fold (U87MG CM), ~2.7-fold (IGF-1), and ~7.0-fold (VEGF), respectively, in the treated cells (Figure 3, *B–D*). CIBP-4 (20 nM) blocked both the angiogenic response and the intracellular CatB activity induced by growth factor treatments (Figure 3, *B–D*).

IBP-4 and CIBP-4 Inhibit U87MG Cell Anchorage-Independent Growth

The anchorage-dependent growth of U87MG cells was not affected by either IBP-4 or CIBP-4 (Figure 4*A*). The anchorage-independent growth, measured as the total area per field covered by U87MG

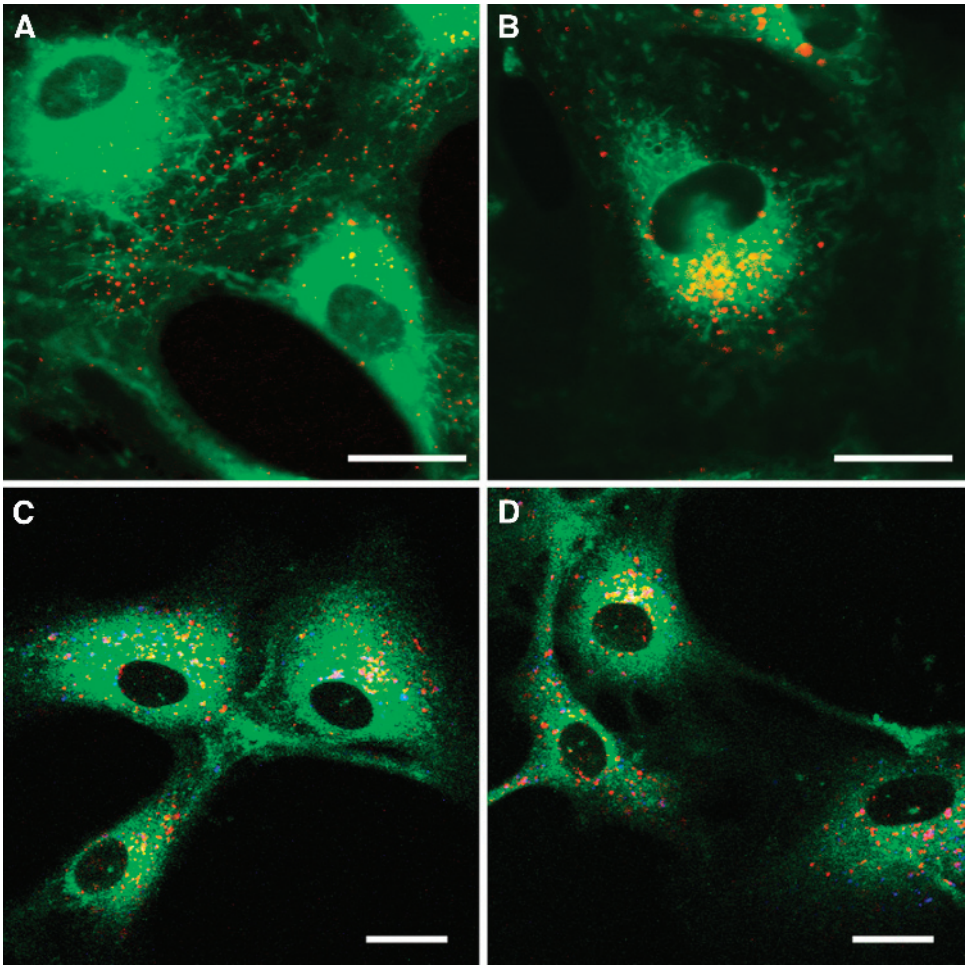

Figure 5. Internalization of recombinant CIBP-4 in HBEC. Confocal microscopy images showing (A and B) internalization of AF647-conjugated CIBP-4 (red) in HBEC counterstained with 500 nM membrane dye DIOC5(3) (green). HBECs were exposed to 200 nM AF647-conjugated CIBP-4 for 30 minutes (A) or 150 minutes (B) at 37°C. (C and D) Co-localization of 200 nM AF647-conjugated CIBP-4 (red) with 150 nM LysoTracker (blue) in HBEC after a 2-hour incubation at 37°C. Cells were counterstained with 10 μM Merocyanine (green). Co-localization of CIBP-4 and LysoTracker appears as pink vesicles. Calibration bar, 25 μm.

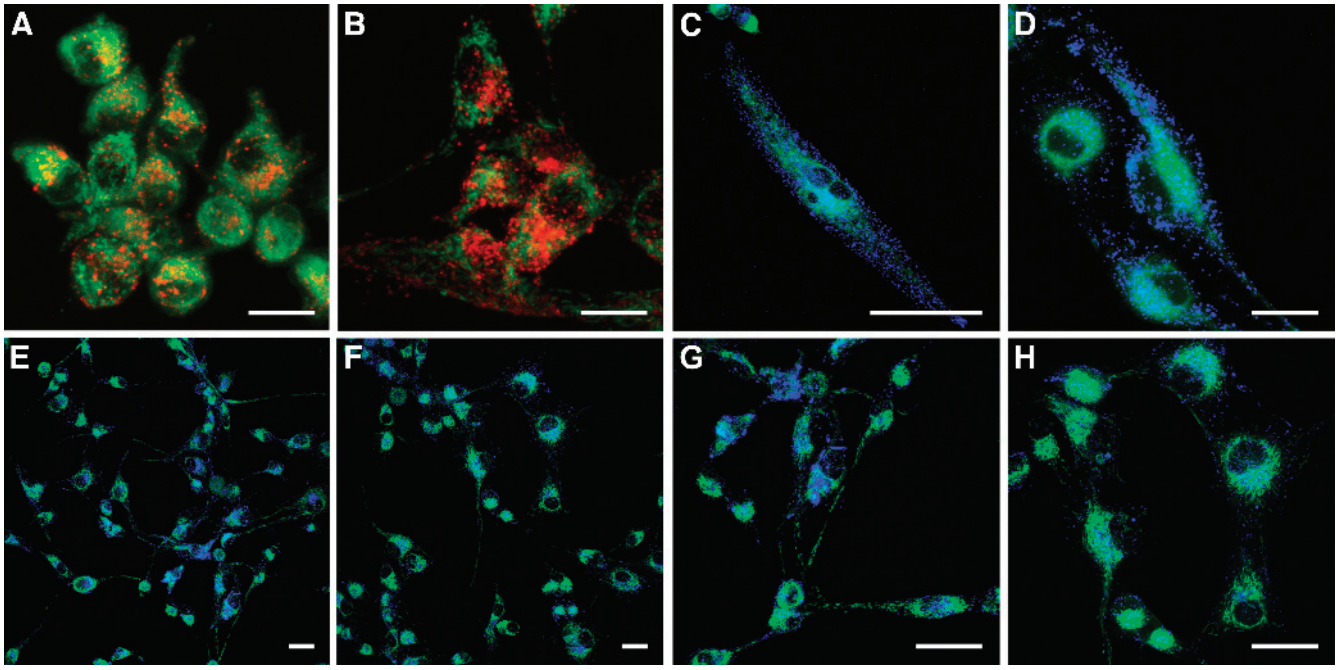

Figure 6. Internalization of recombinant CIBP-4 and its effect on cellular CatB activity in U87MG cells. Confocal microscopy images showing (A and B) internalization of 200 nM AF647-conjugated CIBP-4 (red) in U87MG cells at 90 minutes (A) or 4 hours (B). Cell were counterstained with 500 nM membrane dye DIOC5(3) (green). Cellular CatB activity (blue) in U87MG cells (C–H) in the absence (C, D, E, and G) or presence (F and H) of 200 nM CIBP-4 for 4 hours at 37°C. CatB activity was monitored using Magic Red CatB reagent. Cells were counterstained with 500 nM DIOC5(3) (green). Calibration bar, 25 μm.

colonies grown in soft agar, was significantly reduced by 20 nM IBP-4 (~37%), 20 nM CIBP-4 (~60%), and 500 μM dB-cAMP (~69%, positive control), compared to untreated cells (Figure 4, *B–F*). U87MG cell viability, measured by Alamar Blue, was also significantly reduced by 20 nM IBP-4 (~25%), 20 nM CIBP-4 (~74%), and 500 μM dB-cAMP (~72%; Figure 4*G*). The total number of colonies was not significantly different between untreated and treated cells (data not shown).

CIBP-4 Internalizes and Targets Lysosomal-Like Structures in HBECs

To determine whether CIBP-4 internalizes in HBEC, cells were exposed to AF647-conjugated CIBP-4 (200 nM) for 150 minutes at 37°C in DMEM. Internalization of CIBP-4 in HBEC was visualized as early as 30 minutes, with most of the protein located at the periphery of the cells and in the cell processes (Figure 5*A*). CIBP-4 internalization increased with time (Figure 5, *A* and *B*). By 150 minutes,

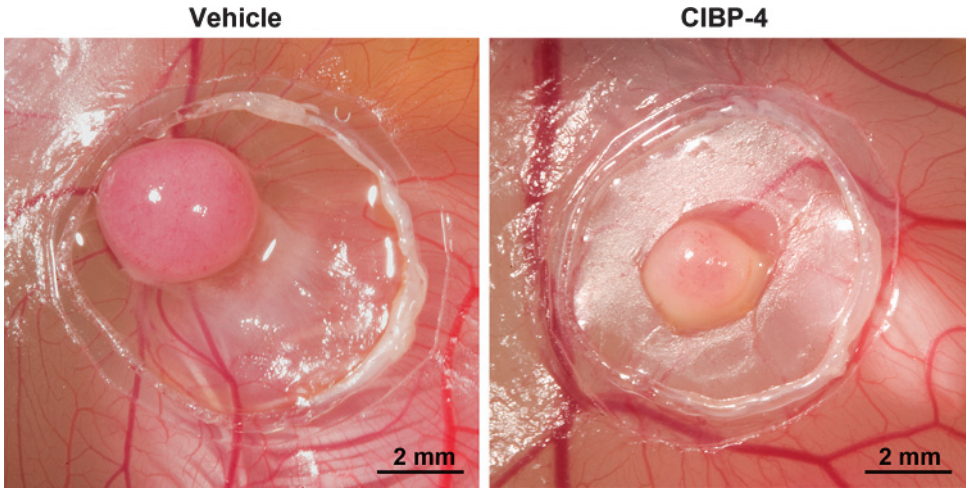

Figure 7. Effects of recombinant CIBP-4 on the growth of U87MG cells grafted on CAM of fertilized eggs. Microphotographs show U87MG tumors 7 days after cell inoculation. Tumors were treated with either DMSO (vehicle) (A) or 108 ng of CIBP-4 (B) for 4 days.

Table 1. Effects of CIBP-4 on U87MG Tumor Growth in CAM Assay.

Weight Range (mg)	0–15		15–20		20–36	
Treatment	Vehicle	CIBP-4	Vehicle	CIBP-4	Vehicle	CIBP-4
Number	7	20	11	11	17	7
Average weight (mg)	10.6 ± 2.3	9.9 ± 3.0	16.7 ± 1.2	17.3 ± 1.7	24.1 ± 3.6	25.9 ± 5.7

Frequency (number) and average weight (mg) of U87MG tumors treated with either DMSO (vehicle) or CIBP-4 (108 ng) in three size groups (small, 0–15 mg; medium, 15–20 mg; large, 20–36 mg).

CIBP-4 was largely localized in vesicle-like structures with predominant perinuclear distribution (Figure 5*B*) as well as along the cellular processes (Figure 5, *C* and *D*). CIBP-4 co-localized (Figure 5, *C* and *D*, pink vesicles) to some extent with the fluorescent acidotropic probe LysoTracker Yellow that selectively labels acidic organelles in the cells, suggesting that a fraction of the internalized CIBP-4 targets lysosomal-like structures in HBEC. The remaining fraction of internalized CIBP-4 was associated with other vesicular structures (Figure 5, *C* and *D*, red vesicles) that likely represent intermediate intracellular trafficking compartments.

CIBP-4 Internalizes in Vesicular-Like Structures and Reduces CatB Activity in U87MG Cells

AF647-conjugated CIBP-4 internalized in U87MG in a time-dependent fashion, with a predominant localization in vesicle-like structures with a perinuclear distribution and along cell processes (Figure 6, *A* and *B*). U87MG cells showed robust CatB activity throughout the cytoplasm and externalized pericellularly into the ECM surrounding the plasma membrane (Figure 6, *C* and *D*). Incubation of the cells with 200 nM CIBP-4 for 90 minutes markedly reduced both pericellular and intracellular CatB activity in U87MG cells (Figure 6, *E*–*H*).

CIBP-4 Inhibits Glioblastoma Tumor Growth in the Experimental Glioma Assay

The ability of CIBP-4 to block U87MG tumor growth was tested in an experimental glioma assay using U87MG cells grafted onto the CAM of fertilized eggs, which form solid and highly vascularized tumors 7 days after inoculation (Figure 7*A*). Tumors treated with CIBP-4 (108 ng) for four consecutive days showed significant ($P < .005$) size reduction (25%) compared to tumors in the vehicle-treated group (Figure 7, *A* and *B*). However, separation of the tumors into three size intervals (small, 0–15 mg; medium, 15–20 mg; large, 20–36 mg) revealed that in the vehicle-treated group, 20% of the tumors fell in the small size interval, 31.4% in the medium size interval, and 48.6% in the large size interval, while in the CIBP-4–treated group, 52.6% of the tumors fell in the small size interval, 29% in the medium size interval, and 18.4% in the small size interval. These data indicate a 2.6-fold shift ($P < .005$, Chi-square test) toward smaller size tumors in the CIBP-4–treated group compared to the vehicle-treated group (Table 1). The average tumor size in each interval was not significantly different between CIBP-4–treated and vehicle-treated groups (Table 1), confirming no artificial bias in the interval limit selection of three size groups.

Pharmacokinetics and Biodistribution of CIBP-4 in a U87MG Xenograft Subcutaneous Tumor Model

The pharmacokinetic profile of CIBP-4 fits well with a biphasic two-compartmental IV bolus model as calculated using WinNonlin Pharmacokinetics software package. CIBP-4 exhibited a β circulation half-life of ~29.3 minutes (Table 2).

Near-infrared *in vivo* optical imaging was used to evaluate the whole body biodistribution of CIBP-4–Cy5.5 in mice-bearing subcutaneous xenograft U87MG-derived tumors. In mice i.v. injected with CIBP-4–Cy5.5, a rapid accumulation (<0.5 hour) of the protein was observed in the tumor, reaching a maximum level after 1 hour (Figure 8*A*). CIBP-4–Cy5.5 also accumulated in the kidneys, a typical clearance route for proteins with a molecular weight <60 kDa. After 1 hour, the fluorescence signal decreased rapidly in the body, consistent with pharmacokinetic profile of the peptide; however, at 24 hours, detectable levels of CIBP-4–Cy5.5 were still present in the tumor and kidney regions.

At the end of imaging protocol (24 hours after injection), tumor sections were analyzed to determine the distribution of CIBP-4–Cy5.5 within the tumor using fluorescent microscopy (Figure 8, *B*–*E*). These studies confirmed that the increased tumor optical signal observed during *in vivo* imaging resulted from the accumulation of CIBP-4–Cy5.5 in the subcutaneous tumors.

The fluorescence signal of injected CIBP-4–Cy5.5 was present throughout the tumor with the exception of the tumor center (Figure 8*B*), which often represents a heavily necrotic area with little or no perfusion. No CIBP-4–Cy5.5 was found in the vasculature 24 hours after injection (Figure 8*C*); however, CIBP-4–Cy5.5 accumulated around presumably "leaky" vessels and diffused into various areas of the tumor (Figure 8*D*). The fluorescent CIBP-4 signal in the tumor cells appeared predominantly localized in perinuclear vesicles (Figure 8*E*) mirroring the peptide distribution pattern observed in the *in vitro* U87MG cellular uptake studies (Figure 6, *A* and *B*).

CIBP-4 Inhibited U87MG Tumor Growth in a Mouse Xenograft Subcutaneous Tumor Model

A subcutaneous U87MG xenograft tumor model in CD-1 nude mice was used to evaluate the therapeutic efficacy of CIBP-4 (Figure 9*A*). CIBP-4 (10 mg/kg) administrated i.v. three times per week resulted in an ~60% reduction in the tumor size in 80% of the animals (Figure 9*B*). Ten percent of the animals showed complete tumor regression, while another 10% were unresponsive to CIBP-4 (data not shown).

Discussion

IGFBPs are multifunctional proteins that can both positively and negatively [35] modulate IGF-induced actions [7,36]. Among the six IGFBPs, IGFBP-4 is the only protein member that has consistently shown to function as a purely inhibitory protein *in vitro* and *in vivo* [8]. These inhibitory actions have been associated with

Table 2. Pharmacokinetic Profile of CIBP-4–Cy5.5.

Parameter Units	CIBP-4
Volume of distribution (ml)	1.0
K10	0.14
K12	0.03
K21	0.03
AUC	1.8
K10 t½ (minutes)	5.0
α½ (minutes)	3.9
β½ (minutes)	29.3
Clearance (ml/min)	0.14

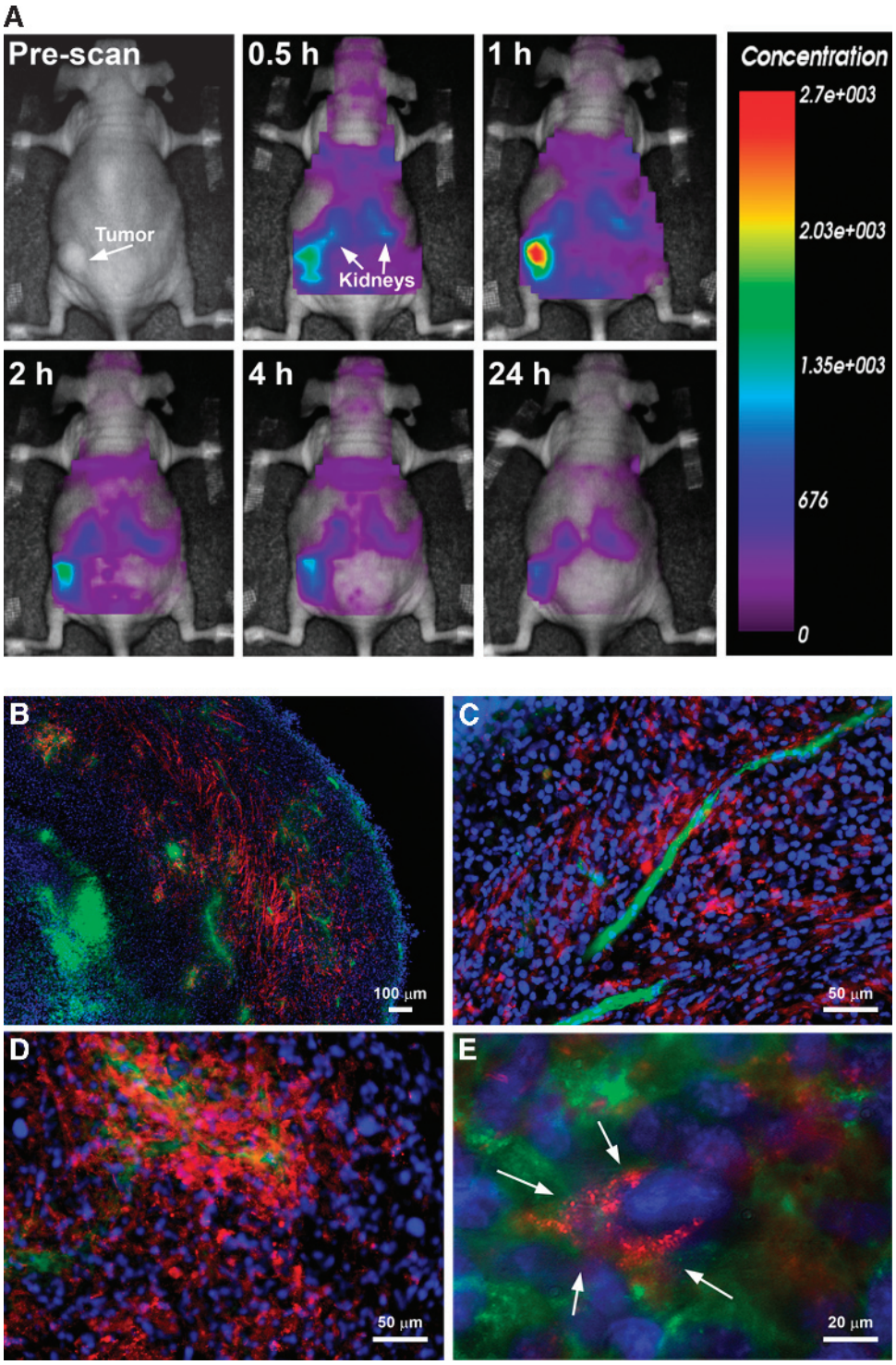

Figure 8. (A) *In vivo* optical images of dorsal whole animal body at various time points (up to 24 hours) after intravenous injection of 100 μg of Cy5.5-labeled CIBP-4 in a subcutaneous tumor-bearing mouse; ×4 magnification (B), ×20 magnification (C and D), and enlarged ×20 (E) fluorescent microscopic images of mouse subcutaneous brain tumor sections obtained 24 hours after intravenous injection of 100 μg of CIBP-4–Cy5.5; CIBP-4–Cy5.5 distribution (red), cell nuclei stained by DAPI (blue), and lectin staining of tumor vessels (green).

IGF-dependent and IGF-independent pathways [37]. In a previous study [10], we identified IGFBP-4 as a protein highly expressed in dB-cAMP–differentiated U87MG cells and showed that IGFBP-4 exerts very potent anti-angiogenic and anti-tumorigenic effects in HBECs and glioblastoma cells, respectively. These two actions were demonstrated to be IGF-independent, although the molecular mechanisms involved are still unknown. Protein sequence analysis indicated the presence of a Tg1 domain in the C-terminal region of IGFBP-4. This Tg1 structural motif is also present as a single or repeated sequence in a variety of structurally and functionally unrelated proteins, generically called thyropins, that however share the ability of inhibiting either cysteine or cation-dependent proteinases [13]. Cysteine

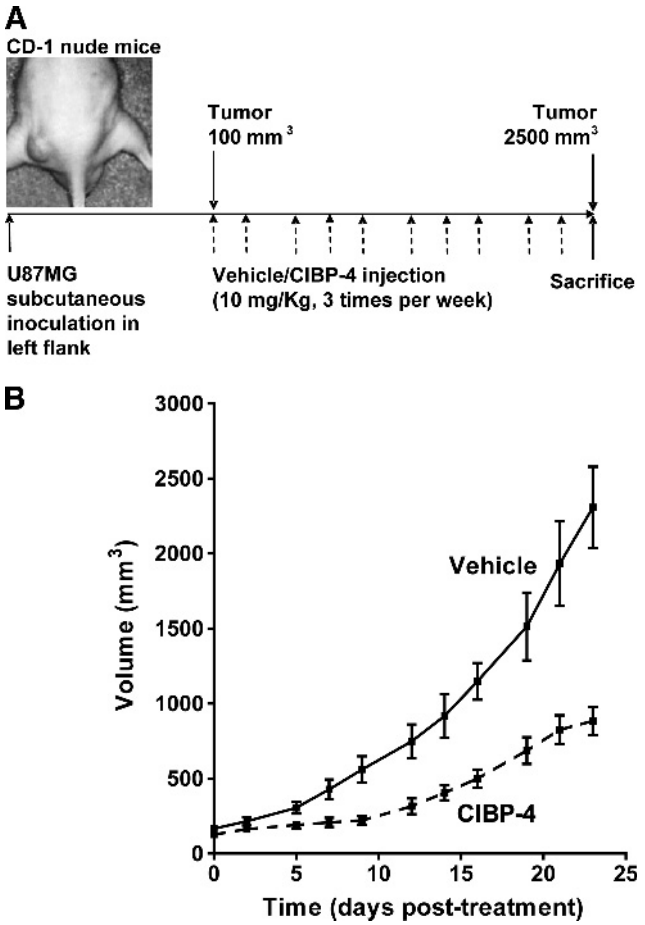

Figure 9. (A) Schematic representation of the animal protocol used to evaluate the therapeutic efficacy of CIBP-4 intravenously injected in CD-1 nude mice-bearing U87MG-derived tumors. (B) Graph representing the growth of subcutaneously implanted U87MG tumors in nude mice after intravenous injection of either vehicle (solid line) or 10 mg/kg CIBP-4 (hatched line) three times per week for a period of 23 days.

cathepsins, particularly CatB, have been shown to be involved in tumor progression and angiogenesis [38,39]. CatB activity is absent in normal brain tissue but overexpressed in glioblastomas, especially in areas of invasion and neovascularization [38,40]. The expression of CatB has been shown to correlate with the degree of histologic malignancy in astrocytomas and with shorter survival in patients [40,41].

To identify the mechanism(s) underlying the IGF-independent anti-angiogenic and anti-tumorigenic activity of IGFBP-4, a C-terminal IGFBP-4 protein fragment (CIBP-4) containing the Tg1 domain was recombinantly produced and its capacity to reduce glioblastoma tumor growth and angiogenesis was tested *in vitro*. CIBP-4 inhibited the angiogenic responses induced by U87MG CM, IGF, and VEGF in HBECs seeded on Matrigel with similar efficacy to that obtained with the full-length protein.

Studies using recombinant CatB protein and a fluorogenic Z-L-R-AMC substrate demonstrated the capacity of CIBP-4 to inhibit CatB activity *in vitro*, supporting the hypothesis that proteins bearing a Tg1 domain in their sequence can act as cysteine proteinase inhibitors. The inhibitory effect of CIBP-4 on CatB activity was even more potent than that exerted by the synthetic CatB inhibitor CA-074 ME at low concentrations.

Confocal microscopy studies showed internalization of AF647-conjugated IGFBP-4 (data not shown) and CIBP-4 in both ECs and U87MG cells targeting perinuclear lysosomal-like structures, which suggests its ability to interact with lysosomal proteases, including CatB. Similarly, IGFBP-5 uptake into perinuclear vesicular structures has been reported in mammary epithelial cells [42]. Some IGFBPs have shown to interact with the cell surface through either $\alpha_5\beta_1$ integrins through their Arg-Gly-Asp sequence (IGFBP-1) [43], the type V transforming growth factor β receptor (IGFBP-3) [44], or ECM proteoglycans through HBDs present in their sequence (IGFBP2, IGFBP-3, IGFBP-5, and IGFBP-6) [4–6]. However, IGFBP-4 lacks consensus HBD and has not as yet been demonstrated to interact with cell membrane surface structures [45]. To the best of our knowledge, our study is the first to report the ability of exogenously applied IGFBP-4 and CIBP-4 proteins to access the intracellular space. This is an important finding and identification of the mechanism(s) of CIBP-4 interaction with cell membrane structures that facilitate its subsequent internalization warrants further investigation.

The ability of exogenous CIBP-4 to reach lysosomal-like structures correlated with its capacity to inhibit intracellular CatB in ECs seeded on Matrigel. During the growth factor–induced capillary-like network formation, a concomitant increase in intracellular CatB activity was observed in HBEC undergoing tubulogenesis. These results support previous *in vitro* [21,46,47] and *in vivo* [48,49] studies, indicating that CatB plays an important role in the process of angiogenesis. Furthermore, both the growth factor–induced angiogenic phenotype and the intracellular CatB activity in ECs were effectively inhibited by CIBP-4.

During tubulogenesis, degradation of the basement membrane by proteolytic enzymes has been considered the principal mechanism to facilitate cell migration, invasion, and capillary tube formation [21]. However, recent studies using quenched fluorescent protein substrates in living cells showed that degradation of ECM protein by CatB can occur extracellularly and intracellularly in both lysosomal-like structures and caveolin-1–containing vesicles [21,47]. Moreover, inhibitors that block both intracellular and extracellular CatB activities are more effective in reducing angiogenesis *in vitro* than those targeting the extracellular CatB fraction alone [21].

Confocal microscopy studies in U87MG cells also demonstrated that CIBP-4 can internalize into the glioblastoma cells and accumulate in perinuclear lysosomal-like structures. CatB activity in U87MG cells was abundant and highly spread throughout the cell body, with a large amount of this activity being localized pericellularly and along the processes. Incubation of U87MG cells with CIBP-4 resulted in a potent silencing/reduction of both pericellular and intracellular CatB activities and a significant inhibition of tumor colony formation in soft agar.

Using an experimental glioma assay, U87MG cells grafted onto the CAM of fertilized eggs, we demonstrated that ectopic application of CIBP-4 for 4 days after tumor cell implantation induced a significant shift toward smaller-sized and less vascularized tumors compared to the nontreated group.

Biodistribution analysis of Cy5.5-labeled CIBP-4 i.v. injected in mice-bearing xenograft subcutaneous tumors showed that the protein reaches and accumulates in the tumor, while it clears rapidly from the rest of the organs. Histologic evaluation of the tumors indicated that CIBP-4–Cy5.5 internalizes into glioblastoma cells and targets perinuclear vesicular structures in a similar fashion to that observed in U87MG cell cultures exposed to CIBP-4.

Efficacy studies in this same animal model demonstrated that CIBP-4 significantly reduces (~60%) tumor growth when administrated i.v. at 10 mg/kg, three times per week. This strong inhibition occurs despite the relatively short half-life (~20 minutes) of CIBP-4 in circulation, suggesting that strategies to increase its half-life may enhance the therapeutic effect of the protein.

This study identifies a novel function for IGFBP-4 as a potent CatB inhibitor and localizes this activity to the C-terminal fragment of the protein containing a Tg1 domain. It also highlights the ability of CIBP-4 to block the angiogenic and tumorigenic activity of glioblastoma cells both *in vitro* and *in vivo*.

Although the proteolytic network that modulates tumor growth and metastasis involves a large number of protease interactions, CatB is emerging as one of the most prominent players [50]. CatB is not only present in tumor cells but also in ECs and macrophages of primary tumors of the central nervous system (CNS) [23]. Overexpression of CatB mRNA transcripts and protein has been identified in human glioma cell lines and biopsy samples and correlates with the malignant progression of gliomas from astrocytomas to glioblastoma multiforme [38,51]. Glioblastoma cell invasion can be significantly inhibited by synthetic inhibitors (K1102, K11017, K11026, K11050, and E64) that are selective for a high spectrum of cysteine proteases, including CatB [52,53], and by inhibitors capable of selectively blocking both intracellular (Ca074 ME) and extracellular (Ca074) CatB activities [54,55]. Furthermore, glioblastoma cells transfected with antisense CatB cDNA exhibit reduced invasion capacity and motility *in vitro* [56] and tumor growth invasion *in vivo* [20,57] compared to the nontreated cells.

At the vascular level, high expression of CatB has been detected in ECs of brain tumors [51] and specifically associated with EC proliferation in regions of tumor infiltration into the adjacent normal brain [58]. Consistent with our findings with CIBP-4, inhibition of CatB activity has been shown to block CLT formation in Matrigel [21,48] as well as angiogenesis in animal models [48,49].

The increase in CatB expression at the invasive edge is not limited to the tumor cells and ECs but is also present in fibroblasts and invading macrophages [59]. CatB has been detected in macrophages surrounding vessels that were located adjacent to necrotic areas [23]. Tumor-associated macrophages have been extensively studied and shown to be a major contributor in tumor progression [60] and angiogenesis.

The prominent role of CatB in tumor progression is underscored by its activation in a variety of cells present within the tumor as well as by its demonstrated role in multiple tumor-promoting cellular processes. CatB has been shown to facilitate the dissemination of cancer cells through degradation of components of the ECM, such as collagen, laminin, and fibronectin [18]. In addition, it contributes to the initiation of the proteolytic cascade that involves 1) direct activation of MMPs such as collagenase-1 and stromelysin [61], 2) activation of the urokinase plasminogen activator/plasminogen activator/plasmin pathway that ultimately activates latent transforming growth factor–β and MMPs [62], and 3) inactivation of tissue inhibitors of metalloproteinases (TIMP-1 and TIMP-2), which in turn enhances the activity of MMPs [63]. Moreover, during proteolytic breakdown of ECMs, some ECM-bound growth factors such as basic fibroblast growth factor, epidermal growth factor, transforming growth factor–β, IGF-I, and VEGF may be liberated, thereby promoting growth effects in tumor and stroma cells.

These studies highlight the potential benefit of anti-CatB therapies, including the use of CIBP-4, in reducing tumor progression, metastasis, and angiogenesis. Evaluation of CIBP-4 efficacy in combination with chemotherapy or radiotherapy may prove useful for the treatment of tumors in which CatB activity is highly increased, such a glioblastoma and pancreatic tumors [38,64].

Acknowledgments

The authors thank Edmund Ziomek for the conjugation of CIBP-4 with AF647 and Tom Devecseri for the acquisition of the CAM experimental glioma photographs and image processing.

References

[1] Firth SM and Baxter RC (2002). Cellular actions of the insulin-like growth factor binding proteins. *Endocr Rev* **23**, 824–854.
[2] Baxter RC (1993). Circulating binding proteins for the insulin-like growth factors. *Trends Endocrinol Metab* **4**, 91–96.
[3] Murphy LJ (1998). Insulin-like growth factor-binding proteins: functional diversity or redundancy? *J Mol Endocrinol* **21**, 97–107.
[4] Booth BA, Boes M, Andress DL, Dake BL, Kiefer MC, Maack C, Linhardt RJ, Bar K, Caldwell EE, Weiler J, et al. (1995). IGFBP-3 and IGFBP-5 association with endothelial cells: role of C-terminal heparin binding domain. *Growth Regul* **5**, 1–17.
[5] Fowlkes JL and Serra DM (1996). Characterization of glycosaminoglycan-binding domains present in insulin-like growth factor-binding protein-3. *J Biol Chem* **271**, 14676–14679.
[6] Russo VC, Bach LA, Fosang AJ, Baker NL, and Werther GA (1997). Insulin-like growth factor binding protein-2 binds to cell surface proteoglycans in the rat brain olfactory bulb. *Endocrinology* **138**, 4858–4867.
[7] Mohan S and Baylink DJ (2002). IGF-binding proteins are multifunctional and act via IGF-dependent and -independent mechanisms. *J Endocrinol* **175**, 19–31.
[8] Zhou R, Diehl D, Hoeflich A, Lahm H, and Wolf E (2003). IGF-binding protein-4: biochemical characteristics and functional consequences. *J Endocrinol* **178**, 177–193.
[9] Ceda GP, Fielder PJ, Henzel WJ, Louie A, Donovan SM, Hoffman AR, and Rosenfeld RG (1991). Differential effects of insulin-like growth factor (IGF)-I and IGF-II on the expression of IGF binding proteins (IGFBPs) in a rat neuroblastoma cell line: isolation and characterization of two forms of IGFBP-4. *Endocrinology* **128**, 2815–2824.
[10] Moreno MJ, Ball M, Andrade MF, McDermid A, and Stanimirovic DB (2006). Insulin-like growth factor binding protein-4 (IGFBP-4) is a novel anti-angiogenic and anti-tumorigenic mediator secreted by dibutyryl cyclic AMP (dB-cAMP)-differentiated glioblastoma cells. *Glia* **53**, 845–857.
[11] Contois LW, Nugent DP, Caron JM, Cretu A, Tweedie E, Akalu A, Liebes L, Friesel R, Rosen C, Vary C, et al. (2012). Insulin-like growth factor binding protein-4 differentially inhibits growth factor-induced angiogenesis. *J Biol Chem* **287**, 1779–1789.
[12] Novinec M, Kordis D, Turk V, and Lenarcic B (2006). Diversity and evolution of the thyroglobulin type-1 domain superfamily. *Mol Biol Evol* **23**, 744–755.
[13] Lenarcic B and Bevec T (1998). Thyropins—new structurally related proteinase inhibitors. *Biol Chem* **379**, 105–111.
[14] Turk V, Turk B, Guncar G, Turk D, and Kos J (2002). Lysosomal cathepsins: structure, role in antigen processing and presentation, and cancer. *Adv Enzyme Regul* **42**, 285–303.
[15] Joyce JA, Baruch A, Chehade K, Meyer-Morse N, Giraudo E, Tsai FY, Greenbaum DC, Hager JH, Bogyo M, and Hanahan D (2004). Cathepsin cysteine proteases are effectors of invasive growth and angiogenesis during multistage tumorigenesis. *Cancer Cell* **5**, 443–453.
[16] Mai J, Sameni M, Mikkelsen T, and Sloane BF (2002). Degradation of extracellular matrix protein tenascin-C by cathepsin B: an interaction involved in the progression of gliomas. *Biol Chem* **383**, 1407–1413.
[17] Lah TT, Buck MR, Honn KV, Crissman JD, Rao NC, Liotta LA, and Sloane BF (1989). Degradation of laminin by human tumor cathepsin B. *Clin Exp Metastasis* **7**, 461–468.
[18] Buck MR, Karustis DG, Day NA, Honn KV, and Sloane BF (1992). Degradation of extracellular-matrix proteins by human cathepsin B from normal and tumour tissues. *Biochem J* **282**(pt 1), 273–278.
[19] Skrzydlewska E, Sulkowska M, Koda M, and Sulkowski S (2005). Proteolytic-antiproteolytic balance and its regulation in carcinogenesis. *World J Gastroenterol* **11**, 1251–1266.

[20] Mohanam S, Jasti SL, Kondraganti SR, Chandrasekar N, Lakka SS, Kin Y, Fuller GN, Yung AW, Kyritsis AP, Dinh DH, et al. (2001). Down-regulation of cathepsin B expression impairs the invasive and tumorigenic potential of human glioblastoma cells. *Oncogene* **20**, 3665–3673.

[21] Premzl A, Turk V, and Kos J (2006). Intracellular proteolytic activity of cathepsin B is associated with capillary-like tube formation by endothelial cells *in vitro*. *J Cell Biochem* **97**, 1230–1240.

[22] Wang M, Tang J, Liu S, Yoshida D, and Teramoto A (2005). Expression of cathepsin B and microvascular density increases with higher grade of astrocytomas. *J Neurooncol* **71**, 3–7.

[23] Strojnik T, Kos J, Zidanik B, Golouh R, and Lah T (1999). Cathepsin B immunohistochemical staining in tumor and endothelial cells is a new prognostic factor for survival in patients with brain tumors. *Clin Cancer Res* **5**, 559–567.

[24] Cass B, Pham PL, Kamen A, and Durocher Y (2005). Purification of recombinant proteins from mammalian cell culture using a generic double-affinity chromatography scheme. *Protein Expr Purif* **40**, 77–85.

[25] Shi C, Shin YO, Hanson J, Cass B, Loewen MC, and Durocher Y (2005). Purification and characterization of a recombinant G-protein-coupled receptor, *Saccharomyces cerevisiae* Ste2p, transiently expressed in HEK293 EBNA1 cells. *Biochemistry* **44**, 15705–15714.

[26] Durocher Y, Perret S, and Kamen A (2002). High-level and high-throughput recombinant protein production by transient transfection of suspension-growing human 293-EBNA1 cells. *Nucleic Acids Res* **30**, E9.

[27] Pham PL, Perret S, Cass B, Carpentier E, St-Laurent G, Bisson L, Kamen A, and Durocher Y (2005). Transient gene expression in HEK293 cells: peptone addition posttransfection improves recombinant protein synthesis. *Biotechnol Bioeng* **90**, 332–344.

[28] Tom R, Bisson L, and Durocher Y (2008). Purification of His-tagged proteins using fractogel-cobalt. *CSH Protoc* **2008**, pdb.prot4980.

[29] Loignon M, Perret S, Kelly J, Boulais D, Cass B, Bisson L, Afkhamizarreh F, and Durocher Y (2008). Stable high volumetric production of glycosylated human recombinant IFNalpha2b in HEK293 cells. *BMC Biotechnol* **8**, 65.

[30] Stanimirovic D, Morley P, Ball R, Hamel E, Mealing G, and Durkin JP (1996). Angiotensin II-induced fluid phase endocytosis in human cerebromicrovascular endothelial cells is regulated by the inositol-phosphate signaling pathway. *J Cell Physiol* **169**, 455–467.

[31] Freitas-Andrade M, Carmeliet P, Stanimirovic DB, and Moreno M (2008). VEGFR-2-mediated increased proliferation and survival in response to oxygen and glucose deprivation in PlGF knockout astrocytes. *J Neurochem* **107**, 756–767.

[32] Hagedorn M, Javerzat S, Gilges D, Meyre A, de Lafarge B, Eichmann A, and Bikfalvi A (2005). Accessing key steps of human tumor progression *in vivo* by using an avian embryo model. *Proc Natl Acad Sci USA* **102**, 1643–1648.

[33] Pen A, Durocher Y, Slinn J, Rukhlova M, Charlebois C, Stanimirovic DB, and Moreno MJ (2011). Insulin-like growth factor binding protein 7 exhibits tumor suppressive and vessel stabilization properties in U87MG and T98G glioblastoma cell lines. *Cancer Biol Ther* **12**, 634–646.

[34] Iqbal U, Albaghdadi H, Luo Y, Arbabi M, Desvaux C, Veres T, Stanimirovic D, and Abulrob A (2010). Molecular imaging of glioblastoma multiforme using anti-insulin-like growth factor-binding protein-7 single-domain antibodies. *Br J Cancer* **103**, 1606–1616.

[35] Rechler MM (1993). Insulin-like growth factor binding proteins. *Vitam Horm* **47**, 1–114.

[36] Clemmons DR (1998). Role of insulin-like growth factor binding proteins in controlling IGF actions. *Mol Cell Endocrinol* **140**, 19–24.

[37] Wetterau LA, Moore MG, Lee KW, Shim ML, and Cohen P (1999). Novel aspects of the insulin-like growth factor binding proteins. *Mol Genet Metab* **68**, 161–181.

[38] Rempel SA, Rosenblum ML, Mikkelsen T, Yan PS, Ellis KD, Golembieski WA, Sameni M, Rozhin J, Ziegler G, and Sloane BF (1994). Cathepsin B expression and localization in glioma progression and invasion. *Cancer Res* **54**, 6027–6031.

[39] Lakka SS, Gondi CS, and Rao JS (2005). Proteases and glioma angiogenesis. *Brain Pathol* **15**, 327–341.

[40] Colin C, Voutsinos-Porche B, Nanni I, Fina F, Metellus P, Intagliata D, Baeza N, Bouvier C, Delfino C, Loundou A, et al. (2009). High expression of cathepsin B and plasminogen activator inhibitor type-1 are strong predictors of survival in glioblastomas. *Acta Neuropathol* **118**, 745–754.

[41] Strojnik T, Kavalar R, Trinkaus M, and Lah TT (2005). Cathepsin L in glioma progression: comparison with cathepsin B. *Cancer Detect Prev* **29**, 448–455.

[42] Jurgeit A, Berlato C, Obrist P, Ploner C, Massoner P, Schmolzer J, Haffner MC, Klocker H, Huber LA, Geley S, et al. (2007). Insulin-like growth factor-binding protein-5 enters vesicular structures but not the nucleus. *Traffic* **8**, 1815–1828.

[43] Jones JI, Gockerman A, Busby WH Jr, Wright G, and Clemmons DR (1993). Insulin-like growth factor binding protein 1 stimulates cell migration and binds to the $\alpha_5\beta_1$ integrin by means of its Arg-Gly-Asp sequence. *Proc Natl Acad Sci USA* **90**, 10553–10557.

[44] Leal SM, Liu Q, Huang SS, and Huang JS (1997). The type V transforming growth factor β receptor is the putative insulin-like growth factor-binding protein 3 receptor. *J Biol Chem* **272**, 20572–20576.

[45] Kelley KM, Oh Y, Gargosky SE, Gucev Z, Matsumoto T, Hwa V, Ng L, Simpson DM, and Rosenfeld RG (1996). Insulin-like growth factor-binding proteins (IGFBPs) and their regulatory dynamics. *Int J Biochem Cell Biol* **28**, 619–637.

[46] Im E, Venkatakrishnan A, and Kazlauskas A (2005). Cathepsin B regulates the intrinsic angiogenic threshold of endothelial cells. *Mol Biol Cell* **16**, 3488–3500.

[47] Cavallo-Medved D, Rudy D, Blum G, Bogyo M, Caglic D, and Sloane BF (2009). Live-cell imaging demonstrates extracellular matrix degradation in association with active cathepsin B in caveolae of endothelial cells during tube formation. *Exp Cell Res* **315**, 1234–1246.

[48] Yanamandra N, Gumidyala KV, Waldron KG, Gujrati M, Olivero WC, Dinh DH, Rao JS, and Mohanam S (2004). Blockade of cathepsin B expression in human glioblastoma cells is associated with suppression of angiogenesis. *Oncogene* **23**, 2224–2230.

[49] Malla RR, Gopinath S, Gondi CS, Alapati K, Dinh DH, Gujrati M, and Rao JS (2011). Cathepsin B and uPAR knockdown inhibits tumor-induced angiogenesis by modulating VEGF expression in glioma. *Cancer Gene Ther* **18**, 419–434.

[50] Mason SD and Joyce JA (2011). Proteolytic networks in cancer. *Trends Cell Biol* **21**, 228–237.

[51] Sivaparvathi M, Sawaya R, Wang SW, Rayford A, Yamamoto M, Liotta LA, Nicolson GL, and Rao JS (1995). Overexpression and localization of cathepsin B during the progression of human gliomas. *Clin Exp Metastasis* **13**, 49–56.

[52] Demchik LL, Sameni M, Nelson K, Mikkelsen T, and Sloane BF (1999). Cathepsin B and glioma invasion. *Int J Dev Neurosci* **17**, 483–494.

[53] Konduri S, Lakka SS, Tasiou A, Yanamandra N, Gondi CS, Dinh DH, Olivero WC, Gujrati M, and Rao JS (2001). Elevated levels of cathepsin B in human glioblastoma cell lines. *Int J Oncol* **19**, 519–524.

[54] Lah TT, Strojnik T, Levicar N, Bervar A, Zajc I, Pilkington G, and Kos J (2000). Clinical and experimental studies of cysteine cathepsins and their inhibitors in human brain tumors. *Int J Biol Markers* **15**, 90–93.

[55] Premzl A, Zavasnik-Bergant V, Turk V, and Kos J (2003). Intracellular and extracellular cathepsin B facilitate invasion of MCF-10A neoT cells through reconstituted extracellular matrix *in vitro*. *Exp Cell Res* **283**, 206–214.

[56] Krueger S, Haeckel C, Buehling F, and Roessner A (1999). Inhibitory effects of antisense cathepsin B cDNA transfection on invasion and motility in a human osteosarcoma cell line. *Cancer Res* **59**, 6010–6014.

[57] Lakka SS, Gondi CS, Yanamandra N, Olivero WC, Dinh DH, Gujrati M, and Rao JS (2004). Inhibition of cathepsin B and MMP-9 gene expression in glioblastoma cell line via RNA interference reduces tumor cell invasion, tumor growth and angiogenesis. *Oncogene* **23**, 4681–4689.

[58] Mikkelsen T, Yan PS, Ho KL, Sameni M, Sloane BF, and Rosenblum ML (1995). Immunolocalization of cathepsin B in human glioma: implications for tumor invasion and angiogenesis. *J Neurosurg* **83**, 285–290.

[59] Castiglioni T, Merino MJ, Elsner B, Lah TT, Sloane BF, and Emmert-Buck MR (1994). Immunohistochemical analysis of cathepsins D, B, and L in human breast cancer. *Hum Pathol* **25**, 857–862.

[60] Yuan A, Chen JJ, and Yang PC (2008). Pathophysiology of tumor-associated macrophages. *Adv Clin Chem* **45**, 199–223.

[61] Eeckhout Y and Vaes G (1977). Further studies on the activation of procollagenase, the latent precursor of bone collagenase. Effects of lysosomal cathepsin B, plasmin and kallikrein, and spontaneous activation. *Biochem J* **166**, 21–31.

[62] Somanna A, Mundodi V, and Gedamu L (2002). Functional analysis of cathepsin B-like cysteine proteases from Leishmania donovani complex. Evidence for the activation of latent transforming growth factor β. *J Biol Chem* **277**, 25305–25312.

[63] Kostoulas G, Lang A, Nagase H, and Baici A (1999). Stimulation of angiogenesis through cathepsin B inactivation of the tissue inhibitors of matrix metalloproteinases. *FEBS Lett* **455**, 286–290.

[64] Bell-McGuinn KM, Garfall AL, Bogyo M, Hanahan D, and Joyce JA (2007). Inhibition of cysteine cathepsin protease activity enhances chemotherapy regimens by decreasing tumor growth and invasiveness in a mouse model of multistage cancer. *Cancer Res* **67**, 7378–7385.